A landmarking protocol for geometric morphometric analysis of squamate endocasts

Rémi Allemand, Camilo López-Aguirre, Jade Abdul-Sater, Waqqas Khalid, Madlen M Lang, Simone Macrì, Nicolas Di-Poï, Gheylen Daghfous, Mary T Silcox

A landmarking protocol for geometric morphometric analysis of squamate endocasts

RÉMI ALLEMAND[1,*], CAMILO LÓPEZ-AGUIRRE[1], JADE ABDUL-SATER[1], WAQQAS KHALID[1], MADLEN M. LANG[1], SIMONE MACRÌ[2], NICOLAS DI-POÏ[2], GHEYLEN DAGHFOUS[3], MARY T. SILCOX[1]

[1]Department of Anthropology, University of Toronto Scarborough, Toronto, ON M1C 1A4, Canada

[2]Institute of Biotechnology, Helsinki Institute of Life Science, University of Helsinki, FI-00014, Helsinki, Finland

[3]Biodôme de Montréal, 4777 av. Pierre-De Coubertin, Montréal, Québec, H1V 1B3T, Canada

** Corresponding author: remi.allemand@gmail.com*

ABSTRACT

Landmark-based geometric morphometrics is widely used to study the morphology of the endocast, or internal mold of the braincase, and the diversity associated with this structure across vertebrates. Landmarks, as the basic unit of such methods, are intended to be points of correspondence, selected depending on the question at hand, whose proper definition is essential to guarantee robustness and reproducibility of results. In this study, 20 landmarks are defined to provide a framework to analyze the morphological variability in squamate endocasts. Ten species representing a cross-section of the diversity of Squamata from both phylogenetic and ecological (i.e., habitat) perspectives were considered in order to select landmarks replicable throughout the entire clade, regardless of the degree of neuroanatomical resolution of the endocast. To assess the precision, accuracy, and repeatability of these newly defined landmarks, both intra- and inter-observer error were investigated. Estimates of measurement error show that most of the landmarks established here are highly replicable, and preliminary results suggest that they capture aspects of endocast shape related to both phylogenetic and ecologic signals. This study provides a basis for further examinations of squamate endocast disparity using landmark-based geometric morphometrics.

Key words: Squamate, endocast, landmark, geometric morphometrics

1. INTRODUCTION

Endocasts, as internal molds of the cranial cavity, are widely used in the fields of paleoneurology and comparative neuroanatomy (e.g., Edinger 1951; Jerison 1973; Bruner et al. 2018). The casts of different internal cranial structures, such as the brain, cranial nerves, and the osseous labyrinth, can be studied in both extant and extinct taxa to provide information about the shape and size of their respective soft-tissue organs. Besides the neurological capabilities that can potentially be inferred from these data, endocasts offer a unique opportunity for assessing neuroanatomical differences among taxa and provide insight into the evolution of these structures (e.g., Watanabe et al. 2021). The advent and development of computed tomography have significantly contributed to the expansion of comparative neuroanatomical studies in both modern and fossil taxa. These techniques are commonly used nowadays as they enable reliable and non-destructive access to virtual endocasts and facilitate the generation of large datasets (e.g., Beyrand et al. 2019; Fernández-Monescillo et al. 2019; Early et al. 2020). At the same time, the development and elaboration of geometric morphometric (GM) methods have provided a powerful toolkit for characterizing endocast morphology, helping to describe, interpret, and analyze endocast variability. These methods, typically involving the use of two- or three-dimensional Cartesian coordinate points (i.e., landmarks; Bookstein 1990, 1991; Dryden and Mardia 1998; Zelditch et al. 2004; Lawing and Polly 2010; Webster and Sheets 2010; Adams et al. 2013), have become widely adopted in endocranial studies (e.g., Aristide et al. 2019; Bertrand et al. 2019; Weisbecker et al. 2021) due to their efficacy in capturing, retaining, and visualizing shape information independently of differences in position, rotation, and isometry (Pereira-Pedro and Bruner 2018).

Ideally, landmarks are (1) homologous anatomical loci that (2) provide adequate coverage of the morphology, (3) can be recognizable on each specimen in the study, (4) do not alter their topological positions relative to other landmarks, and (5) lie within the same plane

for 2D data (Zelditch et al. 2004; Webster and Sheets 2010). Based on these criteria, landmarks are traditionally classified into three types depending on their structural location and how informative the landmarks may be in terms of biological processes and epigenetic factors. (Bookstein 1990, 1991; but see Lele and Richtsmeier 2001 for another classification of landmarks). Type I landmarks, defined as the intersection between different tissue types, are generally the most desirable type of landmark because of their ease of reproducibility and potential for identifying direct biological meaning (e.g., Bookstein 1991; Zelditch et al. 2004). Type II landmarks can be defined as maxima of curvature and are based on geometric evidence. As Type I landmarks may be difficult to identify for certain structures, especially across a broad taxonomic scale, Type II landmarks may provide a better coverage of the morphology and be more useful in term of comparability (Bookstein 1991). Type III landmarks were first defined as extremal points or points that are defined by virtue of information at other locations on that object (e.g., Bookstein 1991; Zelditch et al. 2004). Such a definition originally encompassed semi-landmarks (Cooke and Terhune 2015), but Weber and Bookstein (2011) redefined this system to identify Type III landmarks as "points characterized locally by information from multiple curves and by symmetry". Following this new definition, semi-landmarks were excluded from this category and were instead sorted as Types IV, V, or VI referring to curves, surfaces or constructed semi-landmarks, respectively, the last category including semi-landmarks that do not fit in the two others (Weber and Bookstein 2011; Cooke and Terhune 2015). It is worth noting that the boundaries among these categories are not sharp, and there may be cases in which landmarks lie in intermediate positions, resulting in a lack of consistency in landmark "Type" assignments across studies (Wärmländer et al. 2019). In addition, as little correlation is observed between landmark type and measurement reproducibility (Wärmländer et al. 2019), one type of landmark should not be preferred or excluded *a priori*, and the selection of landmarks should forefront their individual replicability and ability to speak to specific

research hypotheses (Bruner and Ogihara 2018; Pereira-Pedro and Bruner 2018; Wärmländer et al. 2019).

The definition of Type I landmarks in endocranial studies remains rare. Although some of these landmarks have been defined from the triple point between major endocast features (e.g., between the optic lobe, cerebrum, and cerebellum, Gold and Watanabe 2018; Watanabe et al. 2019a), their recognition relies on being able to establish homologous borders between particular structures of the brain, which in turn depends on the degree to which the brain is faithfully reproduced in the endocast, which is highly variable among vertebrates (e.g., Balanoff and Bever 2017). This leaves most of the points that can be defined on endocasts as representing surfaces, bosses, and curves so that endocranial studies tend to commonly use Type II landmarks (e.g., Aristide et al. 2016, 2019; Bertrand et al. 2019; Hu et al. 2021). To provide meaningful coverage of the endocast in areas that are difficult to define using traditional landmarks, endocranial studies generally use curve or/and surface semi-landmarks to improve the representation of endocast morphology (e.g., Neubauer et al. 2010; Gold and Watanabe 2018; Lautenschlager et al 2018; Beyrand et al. 2019; Watanabe et al. 2019a; Hu et al. 2021; Segall et al. 2021; Weisbecker et al. 2021). Such methods require some caution when interpreting the results, as semi-landmarks imply several methodological choices (e.g., Gunz and Mitteroecker 2013; Gonzalez et al. 2016; Cardini 2020) that may impact their true representation of the real anatomical elements and so limit biological inferences (Bruner and Ogihara 2018; Pereira-Pedro and Bruner 2018). Nonetheless, the use of semi-landmarks, associated with traditional landmarks that are essential as anchor points, can be extremely helpful to characterize the morphology of endocast areas.

The main goal of this study is to use landmark-based geometric morphometric methods to compare the endocast morphology of members of Squamata (snakes and “lizards”). As a first step, landmarks already established in endocranial studies were surveyed to select ones that

could be used in Squamata. In particular, numerous landmarks have been defined for mammals (e.g., Neubauer et al. 2010; Ahrens 2014; Danilo et al. 2015; Bertrand et al. 2019; Barbeito-Andrés et al. 2020; Fontoura et al. 2020; Weisbecker et al. 2021) and birds (e.g., Carril et al. 2016; Marugán-Lobón et al. 2016; Gold and Watanabe et al. 2018; Hu et al. 2021; Watanabe et al. 2021). However, as the morphology of the endocast in these two clades differs markedly from that observed in squamates (e.g., Allemand et al. 2017), the definitions of some of these landmarks are not transferable to the squamate endocast (e.g., landmark 4 in non-passerine birds "*Most rostral point of the eminentia sagittalis*", Carril et al. 2016; landmark 24 in rodents "Caudal-most point on neocortex", Bertrand et al. 2019). Additionally, as landmarks characterizing endocasts in mammals and birds, as well as in crocodilians (e.g., Fabbri et al. 2017; Beyrand et al. 2019; Watanabe et al. 2019a; Hu et al. 2021), are generally defined from the corresponding brain structure they reflect (e.g., "*Dorsal most junction point of cerebrum and optic lobe*", Watanabe et al. 2019a), such definitions can be problematic and unreproducible in squamates, in which those anatomical locations cannot always be identified because of the less close correspondence to the brain in some of these taxa (e.g., *Uropeltis woodmasoni*, Olori 2010; *Typhlophys squamosus*, Allemand et al. 2017). Segall et al. (2021) offers an alternative to these limits by placing landmarks on the bones surrounding the endocranial cavity in snakes. This technique allows one to indirectly characterize the endocast morphology without considering the neuroanatomical resolution of the endocast. However, as such a method is only performed using endocasts and bones, the correspondence between particular points and key landmarks on the diverse brain morphologies in Squamata (e.g., Macrì et al. 2019) are unaccounted for and may remain incidental. In addition, as the great diversity of squamates is associated with a remarkable variability in cranial anatomy with respect to the morphology of the bones surrounding the endocranial cavity (e.g., Da Silva et al. 2018; Watanabe et al. 2019b), and also in terms of the presence, absence, and variable degrees of fusion of bones and cartilage

(e.g., Ollonen et al. 2018), such a method can be difficult to apply when diverse squamates, other than snakes, are considered.

In view of these difficulties, the present contribution aims to create a set of anatomical landmarks for the assessment of the endocast shape in squamates via geometric morphometric approaches, reproducible through the whole clade, and regardless of the neuroanatomical resolution of the endocast. These points can serve a dual purpose of providing a framework for characterizing endocast shape, and also serving as potential anchor points for future semi-landmark analyses. Because of the complicated nature of squamate endocasts and the difficulties in unambiguously locating associated landmarks, several error analyses were completed in order to evaluate the accuracy and repeatability of these newly defined landmarks.

2. MATERIAL AND METHODS

2. 1. Materials

In order to define replicable landmarks for all squamates, the crania of 10 extant species were selected to include representatives of each major clade within Squamata (see Table 1 and Fig. 1; Pyron et al. 2013; Singhal et al. 2021). As bones surrounding the endocranial cavity may be useful to landmark squamate endocasts, specimens were also selected based on their diverse cranial morphologies (Fig. 1) and to represent a variety of different habitats (see Table 1) that may impact the cranial bone conformation (e.g., Barros et al. 2011; Da Silva et al. 2018). Finally, the dataset includes specimens in which the endocast shows varying degrees of neuroanatomical resolution (Fig. 1).

2. 2. Data acquisition

Computed-tomographic scans of adult squamate heads were obtained from different sources (see Table 1). Eight specimens were sampled from the previously published work of Macrì et

al. (2019) for which scans were performed at the University of Helsinki (Finland) using a Skyscan 1272. A ninth specimen, *Sphaerodactylus caicosensis*, was acquired from the online database MorphoSource (Boyer et al. 2016; http://www.MorphoSource.org/). A tenth specimen, *Thamnophis sirtalis*, was acquired by one of the co-author (GD) and the scan was performed at the European Synchrotron Radiation Facility (ESRF, Grenoble, France) using third-generation synchrotron microtomography on beamlines ID19 and BM5 (resolution between 5.0 and 14.9 µm; reconstructions performed using filtered back-projection algorithm with the ESRF PYHST software).

Image segmentation and visualization were performed using the software Avizo version 2019.1 (Thermo Fisher Scientific, U.S.A.). The segmentation tools of the software were used to manually reconstruct the endocast for each species by segmenting the internal surface of the bones, or of the dura mater when no bones surround the endocranial cavity. Additionally, each bone showing a direct contact with the endocranial space was segmented individually, as was the whole brain, the cranial nerves, and the endosseous labyrinth. All the landmarks were placed on the virtual model and exported using the software Avizo (version 2019.1).

2. 3. Landmark definition and error analysis

The variable neuroanatomical resolutions observed on the endocasts of the specimens studied here, as well as the varying spatial relationships established in Allemand et al. (in press) between the brain and the surrounding cranial structures (i.e., bones, endosseous labyrinth, cranial nerves), have been taken into account to define landmarks reproducible through the whole clade of Squamata.

By following the detailed landmark protocol established in this study (see Supplementary data 1), three of the authors (MML, WK and RA) independently performed 10 landmark-placement trials each on *Blanus*, *Sphaerodactylus* and *Epicrates* (see Supplementary

data 2 for raw coordinates of the 90 replicates across species and observers). The three species were selected in order to illustrate the diverse endocast morphologies occurring in squamates. Familiarity with neuroanatomy and endocast landmarks varied among the observers from a complete novice endocast landmarker (WK) to advanced endocast landmarkers without (MML) or with (RA) knowledge of reptile neuroanatomy. For each species the same reconstruction, based on the same threshold values, was used for all trials, and landmarks were only positioned on the left side. Individual trials were separated by at least one day, and the full series of trials was spread out over more than a month.

To determine whether the number of landmarks defined for squamate endocasts is adequate to fully capture changes in shape and size, we used the *Landmark Sampling Evaluation Curve* (LaSEC) function, developed in the R package 'LaMBDA' (LandMark-Based Data Assessment; Watanabe 2018) on each of the 30 landmarking trials for *Blanus*, *Sphaerodactylus* and *Epicrates* separately, and on the inter-specific dataset including one landmarking trial per specimen for each of the 10 different species studied here (landmarks positioned by the first author, see Supplementary data 3 for the raw coordinates). This approach estimates the fit of a 'parent' landmarking protocol from the original dataset by comparing it with the fit of subsampled landmarking protocols using Procrustes Sum of Squares. The original dataset was subsampled by sequentially adding one landmark at a time starting from three (each addition representing a new subsample), comparing the fit of each subsample to the parent protocol (Watanabe 2018). An optimal landmarking protocol is expected to reach stationarity in its fit before the parental level of complexity is reached.

In order to test the reproducibility of the landmarks, the intra-observer errors were calculated separately for the three observers and for each species, and the observers' data were pooled for each species to get some measure of the inter-observer error. As data were collected from objects in a fixed coordinate system (3D coordinate system of the scanner), no type of

fitting criteria have been used to make comparisons between trials, and the measurement error of the unilateral landmarks were computed directly from the data. The means, variances, and standard deviations were calculated as described in von Cramon-Taubadel et al (2007).

To interpret the errors in individual landmarks into a broader context, the coefficient of variation was used, with the aim of seeing how errors in the placement of landmarks contribute to errors in the inter-landmark distances they define (e.g., Schmidt et al. 2011). The linear distances between landmarks were calculated for each species by using the *interlmkdist* function in the R package 'geomorph' version 4.0 (Baken et al. 2021), and each landmark's standard deviation were divided by the mean of the distances for which that landmark is an endpoint to put the estimates of overall error into perspective.

2. 4. Morphospace distribution

We performed two Generalized Procrustes Analyses (GPA) by using the *gpagen* function in the R package 'geomorph' (Baken et al. 2021) to quantify and visualize differences in endocast morphologies captured by the newly-defined landmarks. First analysis was completed by using the 90 trials, including the 10 repetitions made by the three observers on *Blanus*, *Sphaerodactylus* and *Epicrates*, to investigate the variability caused by the landmarking acquisition. The second analysis was performed on the 10 different species studied here, including one landmarking set per specimen (see Supplementary data 3 for the raw coordinates) in order to explore patterns of major morphological variation in squamate endocasts. For each analysis, we performed a Principal Component Analysis (PCA) using the *gm.prcomp* function in 'geomorph' and we estimated heat maps of landmark shape variation by comparing the minimum and maximum of each PC, using the R package 'landvR' (Guillerme and Weisbecker 2019), to visualize the magnitude of shape variation across principal components (PCs) explained by individual landmarks. Procrustes ANOVAs (PLM) were calculated by using the

procD.lm function of the 'geomorph' package to test patterns of endocast shape variation captured by the landmarks based on different factors of variability depending on analysis: (1) observers, species and number of trials (procD.lm (coords~Observer+Species+Rep)), and (2) groups (i.e., snake, amphisbaenian, or lizard), habitat, and allometry (procD.lm (coords~groups+habitat+log(size)). In addition, phylogenetic Procrustes ANOVAs were computed using the *procD.pgls* function to test patterns of endocast shape variation captured by the landmarks based on habitat and allometry (procD.pgls (coords~habitat+log(size)) after controlling for evolutionary relatedness. The typology of the phylogenetic tree used to run the Phylogenetic Generalized Least Squares model (PGLS) is modified from Pyron et al. 2013.

3. RESULTS

3. 1. Landmark Selection

Twenty landmarks were chosen to capture the morphology of squamate endocasts and defined in order to allow for their reliable and repeatable placement (Fig. 2 and Table 2, see Supplementary data 1 for the complete landmarking protocol). Although the landmarking process was first conceptualized by considering anatomical equivalences across all species, landmarks defined on a purely geometric basis were included to complete the coverage of the squamate endocast. Thus, landmarks 8 (Most ventro-median extent of the endocast at the posterior margin of the optic nerve foramen) and 15 (Dorso-median extent of the endocast between the endosseous labyrinths) do not refer to specific brain regions and reflect only geometric information in all species. Similarly, landmarks 11 (Most lateral extent of the endocast at the anterior end of the anterior semicircular canal) and 12 (Most dorso-median extent of the endocast at the anterior end of the anterior semicircular canal) have only a geometric meaning in the snakes *Epicrates* and *Thamnophis*, as well as in the amphisbaenian *Leposternon*. However, these two landmarks variably reflect the anatomy of the brain in the

snake *Xerotyphlops* and other "lizards" (Allemand et al. in press); specifically, they correspond to the lateral most extent of the optic lobes (landmark 11 in *Lepidothyris*, *Pseudopus*, *Sphaerodactylus*, *Tropidurus*) or to the dorsal limit between the cerebral hemispheres and the optic lobes on the brain (landmark 12 in *Xerotyphlops*, *Blanus*, *Lepidothyris*, *Melanoseps*, *Sphaerodactylus*, *Tropidurus*).

3. 2. Landmarking Accuracy

LaSEC analyses show that the number of landmarks required to capture squamate endocast morphology (shape and centroid size) varies depending on species (Fig. 3a, b, c, e, f, g). Relative to *Epicrates* and *Sphaerodactylus*, the curves obtained from the landmark-placement trials performed for *Blanus* show that fewer landmarks are needed to reach the median fit value of 0.95 (Fig. 3a, e). The addition of certain landmarks shows marked improvement in fit values and indicates that some landmarks are more critical in this species for capturing shape and size information of the endocast. Curves obtained from the landmark-placement trials performed for *Epicrates* (Fig. 3c, g) and *Sphaerodactylus* (Fig. 3d, h) show that, despite the lack of a distinct plateau, the variance in fit values steadily decreases as the landmark sampling approaches the parent dataset. These results suggest that the convergence to the parent dataset is genuine although confirming the authenticity of the asymptotic trajectory requires sampling additional landmarks to extend the sampling curve. LaSEC analyses performed on the inter-specific dataset show that reaching the median fit value of 0.95 requires 10 landmarks of the 20 total landmarks (Fig. 3d, h). Despite the lack of a long plateau, sampling curves for both shape and centroid size indicate that the differences between the variance in fit values diminish to be minute as additional landmarks (11 to 20) are sampled. This suggest that the 20 landmarks defined here were effective in capturing the inter-specific endocast morphological variation across squamates.

3. 3. Intra- and Inter-Observer Errors

Tables 3, 4, and 5 show the measurement error for each landmark for the sampling trials on *Blanus* (Table 3), *Epicrates* (Table 4), and *Sphaerodactylus* (Table 5) for each observer and for the pooled data. In the three tables, the standard deviations (σ) are ranked from most error-prone (#1) to least error-prone (#20). The coefficient of variation (CV) is reported for each landmark as a percentage.

The error associated with the placement of the landmarks differs based on both species and observers. The measurements calculated for *Blanus* show that the landmarks positioned on the cast of the olfactory bulbs and peduncles (landmarks 2, 3, 4) and on the most lateral extent of the cast of the cerebral hemispheres (landmark 9) are among the most error-prone landmarks for at least two of the three observers (Table 3). The coefficients of variation, computed from the average distances that the landmarks define, indicate that the relative errors are high (> 5%) for the three landmarks positioned on the cast of the olfactory bulbs and peduncles (landmarks 2, 3, 4) in two observers (MML and WK). The same landmarks are not associated with high CVs for the third observer (RA) and in fact the CVs are below 5% for all landmarks in the *Blanus* dataset for that observer, indicating a better degree of precision. The landmarks located on the dorsal-most extent of the endocast at the level of the anterior-most extent of the endosseous labyrinth (landmark 12), the cast of the mesencephalic flexure (landmark 14), the dorsal-most extent of the endocast between the endosseous labyrinth (landmark 15), the lateral-most extent of the endocast at the endo-lymphatic foramen (landmark 16), and the ventral-most extent of the posterior rhombencephalic cast (landmark 20), represent the least error-prone landmarks for *Blanus* for at least two of the three observers (Table 3). The coefficients of variation for these landmarks are low (< 2%), suggesting a high degree of precision for each observer. When the pooled data are considered, the three landmarks located on the cast of the

olfactory bulbs and peduncles in *Blanus* (landmarks 2, 3, 4) again show a high relative error (> 10%), whereas other landmarks are below 4%, indicating a high degree of precision and consistency in general.

The measurement errors calculated for *Epicrates* indicate that the landmarks located on the dorso-median extent of the anterior olfactory part of the brain (landmark 3), the posterior margin of the optic nerve foramen (landmark 8), the dorso-median and lateral-most extent of the cast of the cerebral hemispheres (landmarks 9 and 10), the ventral-most extent of the diencephalic cast (landmark 13), and the lateral-most extent of the posterior rhombencephalic cast (landmark 18), constitute the most prone-error landmarks in at least two of the three observers (Table 4). Even these landmarks exhibit a good degree of precision for all observers, however, as all the coefficients of variation are uniformly low (< 5%). The landmarks positioned on both the lateral-most and dorso-median extents of the cast of the anterior cerebral hemispheres (landmarks 5 and 6), the dorsal-most extent of the endocast at the level of the anterior-most extent of the endosseous labyrinth (landmark 12), the cast of the mesencephalic flexure (landmark 14), the dorsal-most extent of the endocast between the endosseous labyrinth (landmark 15), and the ventral-most extent of the posterior rhombencephalic cast (landmark 20), represent the least error-prone landmarks in *Epicrates*. The coefficients of variation calculated for these landmarks are very low (< 2%), indicating a high degree of precision for each observer. The measurement errors for the pooled data show a similar pattern, and the coefficient of variation for all but one of the landmarks is low (< 5%), most being below 3%, indicating a high degree of precision and consistency in general. The only exception is the landmark 11, located on the lateral-most extent of the endocast at the level of the anterior-most extent of the endosseous labyrinth, which was the most error-prone landmark in the pooled data. The somewhat higher coefficient of variation (5.07%) associated to this landmark suggests that

although its placement is consistent within the three observers, its position may differ to some degree between the observers.

The measurement errors calculated for *Sphaerodactylus* (Table 5) indicate that the landmarks located on both the lateral-most and ventro-median extents of the cast of the anterior cerebral hemispheres (landmarks 5 and 7), the posterior margin of the optic nerve foramen (landmark 8), the lateral-most extent of the cast of the cerebral hemispheres (landmark 9), and on the lateral-most extent of the endocast at the level of the anterior-most extent of the endosseous labyrinth (landmark 11), constitute the most error-prone landmarks in at least two of the three observers (Table 5). Of these landmarks, the coefficient of variation is high (> 5%) for only the one located on the lateral-most extent of the cast of the anterior cerebral hemispheres (landmarks 5) in one observer (MML), whereas the same landmark in the two other observers (WK and RA) and other high error-prone landmarks are below 5%, indicating a better degree of precision. In one of the observers (MML), the higher coefficient of variation is calculated for the landmark corresponding to the anterior-most extent of the endocast (landmark 1), despite an intermediate ranking (#10) based on the standard deviation value. As this landmark is involved in the shortest inter-landmark distances, any deviation in its placement will greatly affect the small distances between this landmark and its near neighbors, which is one possible explanation for the higher CV. Among the least error-prone landmarks, the ones positioned on the dorsal-most extent of the endocast at the level of the anterior-most extent of the endosseous labyrinth (landmark 12), the dorsal-most extent of the endocast between the endosseous labyrinth (landmark 15), as well as both the dorsal- and ventral-most extents of the posterior rhombencephalic cast (landmarks 19 and 20) are found in at least two of the three observers. The coefficients of variation for these landmarks are low (< 2%), most being lower than 1%, suggesting a high degree of precision for each observer. The measurement errors for the pooled data show a similar pattern than the intra-observer errors, and the low coefficients

of variation in all landmarks indicates a high degree of precision and consistency in general. Similar to the observation made for one of the observers (MML), landmark 1 (anterior-most extent of the endocast) in the pooled data exhibits a higher coefficient of variation (5.25%) suggesting that its variable position impacts the distances with other landmarks.

3. 4. Morphospace Distribution

3. 4. 1. Landmarking trials for Blanus, Epicrates, and Sphaerodactylus

Principal Components Analysis on the endocast morphology of the 90 trials including *Blanus*, *Sphaerodactylus* and *Epicrates* resulted in the first two PCs of morphospace accounting for 96.7% of shape variance (PC1= 73.7%, PC2= 23%; Fig. 4; see Supplementary data 4 for the variance explained by other PCs). PC1 primarily divides the three species from each other, *Blanus* and *Sphaerodactylus* representing the two extremes whereas *Epicrates* has an intermediate position (Fig. 4). It is clear from the high proportion of variation accounted for by this axis, and the amount of variation between species compared to that within each cluster of trials, that the magnitude of inter-species differences is much higher than the variation among observers. The distribution of species on PC1 is not driven by size, as the two extremes, *Blanus* and *Sphaerodactylus*, both exhibit smaller skull lengths than *Epicrates* (see Table 1). Heat plots of landmark displacement between extreme PC1 shape configurations show that the overall main variation relates to the anterior half of the endocast (Fig. 4c, d). The distribution of species along PC1 is mostly affected by the differences in the relative anterior-posterior elongation of the cast of the olfactory bulbs and peduncles, *Blanus* showing shorter olfactory bulbs and peduncles compared to the elongate ones in *Sphaerodactylus*, whereas *Epicrates* shows an intermediate length. Additionally, the position of the lateral most extent of the cast of the cerebral hemispheres influences the distribution of the three species, with that point occurring more posteriorly in *Blanus* than in *Sphaerodactylus*. In *Epicrates*, the lateral-most extent of the

cast of the cerebral hemispheres is located between these two extremes. The second axis (PC2) separates *Blanus* and *Sphaerodactylus* from *Epicrates* (Fig. 4). Again, the variation being captured here is overwhelmingly related to real differences in endocast shape, rather than the identity of the observer. Similar to PC1, the variation along PC2 mostly relates to the anterior half of the endocast, and the relative width of both the casts of the olfactory bulbs + peduncles and the cerebral hemispheres are critical to the distribution of species (Fig. 4g, h). Thus, these endocast regions appear relatively wider in *Epicrates* than in *Blanus* and *Sphaerodactylus*.

Procrustes ANOVA (PLM) revealed that on the three factors tested (Observer, species, repetition), significant differences are recovered between observers and species, whereas the number of repetitions is not significant (Table 6). Species explained the highest proportion of endocast shape variation (96.1%), whereas observer accounted for 0.4%. Species (Z = 14.27) had the greatest effect on endocast shape variation compared to observer (Z = 2.52).

3. 4. 2. All species

Principal Components Analysis on the endocast morphology of the ten different species of squamates resulted in the two first PCs of morphospace accounting for 71.6% of shape variance (PC1= 58.8%, PC2= 12.8%; Fig. 5, see Supplementary data 5 for the variance explained by other PCs). The variation along the two PCs mostly relates to the anterior half of the endocast. The distribution along PC1 primarily divides the fossorial species, including both burrower and cryptozoic taxa, from those that inhabit other habitats (Fig. 5), and is mostly affected by the morphology of the cast of the olfactory bulbs and peduncles, as well as the position of the lateral most extent of the cast of the cerebral hemispheres. Species on the negative side of PC1 exhibit a relatively shorter and stouter cast of the olfactory bulbs and peduncles (e.g., *Leposternon,* Fig. 5a, b) and the lateral most extent of the cast of the cerebral hemispheres is somewhat at the same level as the pituitary cast, the latter being poorly developed ventrally (Fig. 5c, d). This

differs from the more elongated and gracile olfactory bulbs and peduncles characterizing species on the positive side of PC1 (e.g., *Tropidurus*, Fig. 5e, f), and in which the lateral-most extent of the cast of the cerebral hemispheres is reached more anteriorly than the well distinct pituitary cast. The variation along PC2 mostly relates to the dorso-ventral extension of the endocast and the position of the most ventral extent of the pituitary cast (Fig. 5g, h). On the negative side of PC2, species exhibit a nearly straight endocast in lateral view (e.g., *Epicrates*, Fig. 5i, j), showing no or a weak flexure, and the ventral most extent of the pituitary cast is reached ventral to the cerebral hemispheres. Species on the positive side of PC2 are characterized by a more pronounced cephalic flexure (e.g., *Tropidurus*, Fig. 5e, f), and the posterior part of the endocast shows a more ventral projection relative to the axis of the olfactory bulbs and peduncles. In these species, the ventral-most extent of the pituitary cast is located more posteriorly than the cast of the cerebral hemispheres.

Procrustes ANOVA (PLM) revealed that on the three factors tested (Group, habitat, allometry) without phylogeny, significant differences are recovered between snakes, amphisbaenians and non-amphisbaenian “lizards”, as well as between habitat categories, whereas allometry is not significant (Table 7). Although both group and habitat have an effect on endocast shape variation, Z = 2.33 and Z= 2 respectively, the group category explained the highest proportion of endocast shape variation (42.5%), whereas habitat accounted for 33.2%. When phylogeny is taken into account, Procrustes ANOVA showed that both habitat ($p = 0.068$) and allometry ($p = 0.463$) are not significant (Table 7).

4. DISCUSSION

This study defined twenty landmarks to capture the morphological disparity in squamate endocasts, and established a protocol for collecting the three-dimensional coordinates. The measurements of both the intra- and inter-observer errors demonstrate that the landmarks could

generally be located reliably, although a few landmarks are more difficult to position. Thus, the placement of landmarks 3 “Dorso-median extent of the cast of the olfactory bulbs and peduncles”, and 9 “Lateral-most extent of the cast of the cerebral hemispheres” is more likely to be imprecise in some species. Additionally, the difficulty in positioning some of the landmarks seems to be related to the varying complexity of the endocast shape across species. For example, for the less experienced observers, the morphology of the cast of the olfactory bulbs and peduncles in *Blanus* posed a challenge to the accurate placements of landmarks 2 “Lateral-most extent of the cast of the olfactory bulbs and peduncles”, 3 “Dorso-median extent of the cast of the olfactory bulbs and peduncles”, and 4 “Ventro-median extent of the cast of the olfactory bulbs and peduncles”, whereas the same landmarks in *Epicrates* and *Sphaerodactylus* were able to be located more reliably. The lower level of precision for these landmarks should be taken into account both when deciding which landmarks to collect for a given study and, if these landmarks are employed, during data analysis. Besides the straightforward steps defined in our protocol to locate the landmarks, we recommend using the three different planes (i.e., coronal, sagittal, and transverse) to help the landmarking process and to keep a consistent orientation across specimens. Here, the two endosseous labyrinths (left and right) were segmented for each species and used to orient the coronal plane so as to be perpendicular to the lateral semi-circular canals. The two other planes, sagittal and transverse, were then positioned perpendicular to the coronal plane and to each other. Each time a plane was used to position a landmark, the two other planes were visible only as a line (i.e., being fully perpendicular to the viewer). Such a process, in our opinion, provides a more repeatable method for the placement of landmarks, especially those that showed more variance in their placement.

Despite the variability introduced by different observers, the landmarks defined here were effective in capturing the inter-specific endocast morphological variation across

squamates, allowing for the differentiation of species and major groups. The significant difference reported here between the three major groups (amphisbaenians, lizards, and snakes) suggests that squamate endocast morphologies may reflect a phylogenetic signal. Indeed, the three species of snakes in this study exhibit a linear endocast that differs from the more flexed endocast characterizing lizards. However, as exceptions to such a pattern do exist (e.g., relatively straight endocast in *Blanus*), the recognition of universal patterns in endocast morphology reflecting squamate phylogeny, if existing, remains challenging. The significant difference obtained when comparing the main habitat categories, being only marginally significant when accounting for phylogenetic distances, indicates that the phylogenetic signal in squamate endocranial morphologies may also be coupled with an ecological signal. Such a signal seems particularly evident in fossorial (burrower and cryptozoic) squamates, including here the two amphisbaenians *Leposternon* and *Blanus*, the scincid "lizard" *Melanoseps*, and the snake *Xerotyphlops*. The endocasts in these species show common morphological trends characterized by a relatively shorter and stouter cast of the olfactory bulbs and peduncles, a lateral-most extent of the cast of the cerebral hemispheres being positioned more posteriorly, and an absence or poor differentiation of the pituitary cast, that differ from terrestrial and semi-arboreal species. Similar to previous studies based on snake endocasts and employing different methods (Allemand et al. 2017; Segall et al. 2021), the detection of such phylogenetic and ecologic signals supports the use of the landmarks defined here and may provide a basis for future studies considering the variability in squamate endocasts.

The number of landmarks defined in this study appears sufficient to differentiate the variable endocranial morphologies observed across major squamate lineages. However, our results indicate that we cannot be confident that these 20 landmarks are sufficient for characterizing variation at the intra-specific level. In view of these limitations, endocranial studies at a finer taxonomic scale will potentially benefit from adding extra landmarks that may

not be identifiable throughout squamates but that are particularly relevant to individual groups or specific hypotheses. Additional anatomical landmarks relevant to a particular clade could thus be selected based on structures whose homology is clear within closely related groups but cannot necessarily be identified across all of squamates. In addition, the reproducible set of landmarks defined here could be used for the placement of semi-landmarks in order to improve the representation of the squamate endocast. Indeed, the inherent issues related to landmarks in the underrepresentation of some part of the endocast and the failure to characterize the shape between them may constitute an important challenge and need to be considered. The new points of correspondence defined in this study could be employed as anchor points for sliding curves semi-landmarks, which, in turn, could demarcate the regions for surface sliding semi-landmarks. Such methods are nowadays largely employed in endocranial studies (e.g., Watanabe et al. 2019a; Hu et al. 2021; Segall et al. 2021; Weisbecker et al. 2021), and would help to characterize the relatively featureless surfaces of squamate endocasts by allowing an endocranial comparisons curve-to-curve or surface-to-surface (e.g., Gunz et al. 2005). By providing replicable landmarks for the whole clade Squamata, the current study was, thus, needed as a first step to quantify and analyze the variability in squamate endocast morphologies and should provide a basis for further examinations using landmark-based geometric morphometrics.

5. CONCLUSION

This study established a detailed protocol for the placement of twenty traditional landmarks in order to analyze the morphological disparity of squamate endocasts. Many of the problems associated with the nearly feature-less nature of squamate endocasts have been overcome. We demonstrate that these newly-defined landmarks are replicable and can be accurately positioned across the entire clade. These landmarks form a basis for landmark-based morphometric

geometric studies quantifying morphological aspects of squamate endocasts. Future studies should consider the definition of additional landmarks relevant to particular hypotheses about endocast shape, and the continued refinement of the protocol proposed here.

ACKNOWLEDGEMENTS

Thanks to David Blackburn on MorphoSource for granting access to the micro-diceCT scans of *Sphaerodactylus caicosensis*. We would also like to thank two anonymous reviewers for helpful comments and suggestions that improved the paper.

DATA AVAILABILITY

The endocasts (stl files) used in the study will be made available on MorphoSource in the following project: https://www.morphosource.org/projects/000488393?locale=en

AUTHOR CONTRIBUTIONS

R.A. and M.T.S. designed the overall experimental approach. Micro-CT scans were carried out by S.M., N.D.P., and G.D. R.A. and J.A.S. made the 3D reconstructions. R.A., W.K, and M.L. collected the 3D landmark data. R.A. and C.L-A. performed the geometric morphometric and statistical analyses. R.A. wrote the first draft of the paper, and all co-authors contributed in the form of discussion and critical comments. All authors approved the final version of the paper.

REFERENCES

Adams, D.C., Rohlf, F.J., & Slice, D.E. (2013) A field comes of age: geometric morphometrics in the 21st century. *Hystrix*, 24(1), 7–14. http://dx.doi.org/10.4404/hystrix-24.1–6283

Afsar, M., Çiçek, K., Tayhan, Y., & Tok, C.V. (2016) New records of Eurasian Blind Snake, *Xerotyphlops vermicularis* (Merrem, 1820) from the Black Sea region of Turkey and its updated distribution. *Biharean Biologist*, 10(2), 98–103

Ahrens, H.E. (2014) Morphometric study of phylogenetic and ecologic signals in procyonid (Mammalia: Carnivora) endocasts. *The Anatomical Record*, 297(12), 2318–2330. https://doi.org/10.1002/ar.22996

Akani, G.C., Capizzi, D., & Luiselli, L. (2002) Community ecology of scincid lizards in a swamp rainforest of South-Eastern Nigeria. *Russ. J. Herpetol*. 9, 125–134

Allemand, R., Boistel, R., Daghfous, G., Blanchet, Z., Cornette, R., Bardet, N., Vincent, P., & Houssaye, A. (2017) Comparative morphology of snake (Squamata) endocasts: evidence of phylogenetic and ecological signals. *Journal of anatomy*, 231(6), 849–868. https://doi.org/10.1111/joa.12692

Allemand, R., Abdul-Sater, J., Macrì, S., Di-Poï, N., Daghfous, G., & Silcox, M.T. (in press) Endocast, brain and bones: correspondences and spatial relationships in squamates. The Anatomical Record.

Andrade-Junior, A., França, M.S., Sudré, V., & Passos, P. (2020) Are there threatened snakes at the end of the rainbow? Notes on the distribution and morphology of *Epicrates cenchria*, Rainbow Boa, in the Brazilian Atlantic Forest. *Cuadernos de Herpetología*, 34(2), 299–304. https://doi.org/10.31017/CdH.2020.(2019-030)

Aristide, L., Dos Reis, S.F., Machado, A.C., Lima, I., Lopes, R.T., & Perez, S.I. (2016) Brain shape convergence in the adaptive radiation of New World monkeys. *Proceedings of the*

National Academy of Sciences, 113(8), 2158–2163. https://doi.org/10.1073/pnas.1514473113

Aristide, L., Strauss, A., Halenar-Price, L.B., Gilissen, E., Cruz, F.W., Cartelle, C., Rosenberger, A.L., Lopes, R.T., dos Reis, S.F., & Perez, S.I. (2019) Cranial and endocranial diversity in extant and fossil atelids (Platyrrhini: Atelidae): A geometric morphometric study. *American journal of physical anthropology*, 169(2), 322–331. https://doi.org/10.1002/ajpa.23837

Baken, E.K., Collyer, M.L., Kaliontzopoulou, A., & Adams, D.C. (2021) geomorph v4. 0 and gmShiny: Enhanced analytics and a new graphical interface for a comprehensive morphometric experience. *Methods in Ecology and Evolution*, 2, 2355–2363. https://doi.org/10.1111/2041-210X.13723

Balanoff, A.M., & Bever, G.S. (2017) The role of endocasts in the studyof brain evolution. In Kaas, J.H., & Striedter, G. (Eds) *Evolution of Nervous Systems*. Oxford: Academic Press, pp. 223–241.

Barbeito-Andrés, J., Bonfili, N., Nogué, J.M., Bernal, V., & Gonzalez, P.N. (2020) Modeling the effect of brain growth on cranial bones using finite-element analysis and geometric morphometrics. Surgical and Radiologic Anatomy, 42(7), 741–748. https://doi.org/10.1007/s00276-020-02466-y

Barros, F.C., Herrel, A., & Kohlsdorf, T. (2011) Head shape evolution in Gymnophthalmidae: does habitat use constrain the evolution of cranial design in fossorial lizards?. *Journal of Evolutionary Biology*, 24(11), 2423–2433. https://doi.org/10.1111/j.1420-9101.2011.02372.x

Bertrand, O.C., San Martin-Flores, G., & Silcox, M.T. (2019) Endocranial shape variation in the squirrel-related clade and their fossil relatives using 3D geometric morphometrics:

contributions of locomotion and phylogeny to brain shape. *Journal of Zoology*, 308(3), 197–211. https://doi.org/10.1111/jzo.12665

Beyrand, V., Voeten, D.F., Bureš, S., Fernandez, V., Janáček, J., Jirák, D., Rauhut, O., & Tafforeau, P. (2019) Multiphase progenetic development shaped the brain of flying archosaurs. Scientific reports, 9(10807). https://doi.org/10.1038/s41598-019-46959-2

Bookstein, F.L. (1990) Introduction to methods for landmark data. In: Rohlf, F.J., & Bookstein, F.L. (Eds.) *Proceedings of the Michigan Morphometrics Workshop*. The University of Michigan Museum of Zoology, Ann Arbor, pp. 215–226.

Bookstein, F.L. (1991) *Morphometric tools for landmark data: Geometry and biology*. Cambridge, UK: Cambridge University Press, p. 435.

Boyer, D.M., Gunnell, G.F., Kaufman, S., & McGeary, T.M. (2016) Morphosource: archiving and sharing 3-D digital specimen data. *The Paleontological Society Papers*, 22, 157–181. https://doi.org/10.1017/scs.2017.13

Bruner, E., & Ogihara, N. (2018) Surfin'endocasts: The good and the bad on brain form. *Palaeontologia Electronica*, 21.1.1A, 1–10. https://doi.org/10.26879/80

Bruner, E., Ogihara, N., & Tanabe, H.C. (2018) *Digital Endocasts*. Tokyo, Japan:Springer, p. 289.

Burger, J., Jeitner, C., Jensen, H., Fitzgerald, M., Carlucci, S., Shukla, S., Burke, S., Ramos, R., & Gochfeld, M. (2004) Habitat use in basking Northern water (*Nerodia sipedon*) and Eastern garter (*Thamnophis sirtalis*) snakes in urban New Jersey. *Urban Ecosystems*, 7(1), 17–27

Cardini, A. (2020) Less tautology, more biology? A comment on "high-density" morphometrics. *Zoomorphology*, 139(4), 513–529. https://doi.org/10.1007/s00435-020-00499-w

Carril, J., Tambussi, C.P., Degrange, F.J., Benitez Saldivar, M.J., & Picasso, M.B.J. (2016) Comparative brain morphology of Neotropical parrots (Aves, Psittaciformes) inferred from virtual 3D endocasts. *Journal of anatomy*, 229(2), 239-251. https://doi.org/10.1111/joa.12325

Cooke, S.B., & Terhune, C.E. (2015) Form, function, and geometric morphometrics. *The Anatomical Record*, 298(1), 5–28. https://doi.org/10.1002/ar.23065

Danilo, L., Remy, J., Vianey-Liaud, M., Mérigeaud, S., & Lihoreau, F. (2015). Intraspecific variation of endocranial structures in extant Equus: a prelude to endocranial studies in fossil equoids. *Journal of Mammalian Evolution*, 22(4), 561–582. https://doi.org/10.1007/s10914-015-9293-x

Da Silva, F.O., Fabre, A.C., Savriama, Y., Ollonen, J., Mahlow, K., Herrel, A., Müller, J., & Di-Poï, N. (2018) The ecological origins of snakes as revealed by skull evolution. *Nature Communications*, 9(1), 1-11. https://doi.org/10.1038/s41467-017-02788-3

Dryden L.L., & Mardia, K.V. (1998) *Statistical shape analysis*. New York: John Wiley and Sons, p. 376.

Early, C.M., Iwaniuk, A.N., Ridgely, R.C., & Witmer, L.M. (2020) Endocast structures are reliable proxies for the sizes of corresponding regions of the brain in extant birds. *Journal of Anatomy*, 237(6), 1162–1176. https://doi.org/10.1111/joa.13285

Edinger, T. (1951). The brains of the Odontognathae. Evolution, 5(1), 6–24.

Fabbri, M., Koch, N.M., Pritchard, A.C., Hanson, M., Hoffman, E., Bever, G.S. Amy M. Balanoff, A.M., Morris, Z.S., Field, D.J., Camacho, J., Rowe, T.B., Norell, M.A., Smith, R.M., Abzhanov, A., & Bhullar, B-A.S. (2017) The skull roof tracks the brain during the evolution and development of reptiles including birds. *Nature Ecology & Evolution*, 1(10), 1543–1550. https://doi.org/10.1038/s41559-017-0288-2

Fernández-Monescillo, M., Antoine, P.O., Pujos, F., Rodrigues, H.G., Quispe, B.M., & Orliac, M. (2019) Virtual endocast morphology of Mesotheriidae (Mammalia, Notoungulata, Typotheria): new insights and implications on notoungulate encephalization and brain evolution. *Journal of Mammalian Evolution*, 26(1), 85–100. https://doi.org/10.1007/s10914-017-9416-7

Fontoura, E., Ferreira, J.D., Bubadué, J., Ribeiro, A.M., & Kerber, L. (2020) Virtual brain endocast of Antifer (Mammalia: Cervidae), an extinct large cervid from South America. *Journal of Morphology*, 281(10), 1223–1240. https://doi.org/10.1002/jmor.21243

Gil, M.J., Guerrero, F., & Pérez-Mellado, V. (1993) Observations on morphometrics and ecology in *Blanus cinereus* (Reptilia: Amphisbaenia). *Journal of Herpetology*, 27(2), 205–209.

Gold, M.E.L., & Watanabe, A. (2018) Flightless birds are not neuroanatomical analogs of non-avian dinosaurs. *BMC Evolutionary Biology*, 18(190), 1–11. https://doi.org/10.1186/s12862-018-1312-0

Gonzalez, P.N., Barbeito-Andrés, J., D'Addona, L.A., Bernal, V., & Perez, S.I. (2016) Performance of semi and fully automated approaches for registration of 3D surface coordinates in geometric morphometric studies. *American Journal of Physical Anthropology*, 160(1), 169–178. https://doi.org/10.1002/ajpa.22934

Guillerme, T., & Weisbecker, V. (2019) landvR: Tools for measuring landmark position variation. Available from: https://www.github.com/TGuillerme/landvR/tree/v0.2.Zenodo. https://doi.org/10.5281/zenodo.2620785.

Gunz, P., Mitteroecker, P., & Bookstein, F.L. (2005) Semilandmarks in three dimensions. In: Slice, D.E. (Ed.) *Modern morphometrics in physical anthropology*. Kluwer Academic/Plenum Publishers, New York, pp. 73–98.

Gunz, P., & Mitteroecker, P. (2013) Semilandmarks: a method for quantifying curves and surfaces. *Hystrix, the Italian Journal of Mammalogy*, 24(1), 103–109. https://doi.org/10.4404/hystrix-24.1-62

Hu, K., King, J.L., Romick, C.A., Dufeau, D.L., Witmer, L.M., Stubbs, T.L., Rayfield, E.J., & Benton, M.J. (2021) Ontogenetic endocranial shape change in alligators and ostriches and implications for the development of the non-avian dinosaur endocranium. *The Anatomical Record*, 304(8), 1759–1775. https://doi.org/10.1002/ar.24579

Jerison, H.J. (1973) Evolution of the brain and intelligence. New York: Academic Press, p. 496

Kearney, M. (2003) Systematics of the Amphisbaenia (Lepidosauria: Squamata) based on morphological evidence from recent and fossil forms. *Herpet. Monog.* 17, 1–74.

Lautenschlager, S., Ferreira, G.S., & Werneburg, I. (2018) Sensory evolution and ecology of early turtles revealed by digital endocranial reconstructions. *Frontiers in Ecology and Evolution*, 6, 7. https://doi.org/10.3389/fevo.2018.00007

Lawing, A.M., & Polly, P.D. (2010) Geometric morphometrics: recent applications to the study of evolution and development. *Journal of Zoology*, 280(1), 1–7. https://doi.org/10.1111/j.1469-7998.2009.00620.x

Lele, S.R., & Richtsmeier, J.T. (2001) *An invariant approach to statistical analysis of shapes*. Boca Raton: Chapman & Hall/CRC, p. 328.

Macrì, S., Savriama, Y., Khan, I., & Di-Poï, N. (2019) Comparative analysis of squamate brains unveils multi-level variation in cerebellar architecture associated with locomotor specialization. Nature Communications, 10(1), 1–16. https://doi.org/10.1038/s41467-019-13405-w

Malonza, P.K., & Bwong, B.A. (2011) Life history notes on loveridge's limbless skink *Melanoseps loveridgei* Brygoo & Roux-Esteve, 1981 (Sauria: Scincidae: Feylininae). *Herpetotropicos* 5, 115–117

Marugán-Lobón, J., Watanabe, A., & Kawabe, S. (2016) Studying avian encephalization with geometric morphometrics. *Journal of anatomy*, 229(2), 191–203. https://doi.org/10.1111/joa.12476

Neubauer, S., Gunz, P., & Hublin, J.J. (2010) Endocranial shape changes during growth in chimpanzees and humans: a morphometric analysis of unique and shared aspects. Journal of Human Evolution, 59(5), 555–566. https://doi.org/10.1016/j.jhevol.2010.06.011

Ollonen, J., Da Silva, F.O., Mahlow, K., & Di-Poï, N. (2018) Skull development, ossification pattern, and adult shape in the emerging lizard model organism *Pogona vitticeps*: a comparative analysis with other squamates. *Frontiers in Physiology*, 9(278). https://doi.org/10.3389/fphys.2018.00278

Olori, J.C. (2010) Digital endocasts of the cranial cavity and osseous labyrinth of the burrowing snake *Uropeltis woodmasoni* (Alethinophidia: Uropeltidae). *Copeia*, 2010(1), 14–26. https://doi.org/10.1643/CH-09-082

Pereira-Pedro, A.S., & Bruner, E. (2018) Landmarking endocasts. In Bruner, E., Ogihara, N., & Tanabe, H.C. (Eds) *Digital endocasts*. Tokyo, Japan:Springer, pp. 127–142.

Pyron, R.A., Burbrink, F.T., & Wiens, J.J. (2013) A phylogeny and revised classification of Squamata, including 4161 species of lizards and snakes. BMC Evolutionary Biology, 13(1), 1–54. https://doi.org/10.1186/1471-2148-13-93

Reynolds, R.G. (2011) Status, conservation, and introduction of amphibians and reptiles in the Turks and Caicos Islands, British West Indies. In Hailey, A., Wilson, B.S., & Horrocks, J.A. (Eds.) *Conservation of Caribbean Island Herpetofaunas, Volume 2: Regional Accounts of the West Indies*. BRILL, pp. 377–406.

Scanferla, A. (2016) Postnatal ontogeny and the evolution of macrostomy in snakes. *Royal Society open science*, 3(11), 160612. https://doi.org/10.1098/rsos.160612

Schmidt, J.L., Cole III, T.M., & Silcox, M.T. (2011) A landmark-based approach to the study of the ear ossicles using ultra-high-resolution X-ray computed tomography data. *American journal of physical anthropology*, 145(4), 665–671. https://doi.org/10.1002/ajpa.21543

Segall, M., Cornette, R., Rasmussen, A.R., & Raxworthy, C.J. (2021) Inside the head of snakes: influence of size, phylogeny, and sensory ecology on endocranium morphology. *Brain Structure and Function*, 226(7), 2401–2415. https://doi.org/10.1007/s00429-021-02340-6

Singhal, S., Colston, T.J., Grundler, M.R., Smith, S.A., Costa, G.C., Colli, G.R., Moritz, C., Pyron, R.A., & Rabosky, D.L. (2021) Congruence and conflict in the higher-level phylogenetics of squamate reptiles: an expanded phylogenomic perspective. *Systematic Biology*, 70(3), 542–557. https://doi.org/10.1093/sysbio/syaa054

Siqueira, C.C., Kiefer, M.C., Sluys, M.V., & Rocha, C.F.D. (2013) Variation in the diet of the lizard *Tropidurus torquatus* along its coastal range in Brazil. *Biota Neotropica*, 13, 93–101

Telenchev, I., Simeonovska-Nikolova, D., & Tzonev, R. (2017) Habitat use and activity of European glass lizard, *Pseudopus apodus* (Pallas, 1775), in southeastern Bulgaria. *Turkish Journal of Zoology*, 41(2), 286–293. https://doi.org/10.3906/zoo-1601-3

von Cramon-Taubadel, N., Frazier, B.C., & Lahr, M.M. (2007) The problem of assessing landmark error in geometric morphometrics: theory, methods, and modifications. *American Journal of Physical Anthropology: The Official Publication of the American Association of Physical Anthropologists*, 134(1), 24–35. https://doi.org/10.1002/ajpa.20616

Wärmländer, S.K., Garvin, H., Guyomarc'h, P., Petaros, A., & Sholts, S.B. (2019) Landmark typology in applied morphometrics studies: What's the point?. *The Anatomical Record*, 302(7), 1144–1153. https://doi.org/10.1002/ar.24005

Watanabe, A. (2018) How many landmarks are enough to characterize shape and size variation?. PloS one, 13(6), e0198341. https://doi.org/10.1371/journal.pone.0198341

Watanabe, A., Gignac, P.M., Balanoff, A.M., Green, T.L., Kley, N.J., & Norell, M.A. (2019a) Are endocasts good proxies for brain size and shape in archosaurs throughout ontogeny?. *Journal of Anatomy*, 234(3), 291–305. https://doi.org/10.1111/joa.12918

Watanabe, A., Fabre, A.C., Felice, R.N., Maisano, J.A., Müller, J., Herrel, A., & Goswami, A. (2019b). Ecomorphological diversification in squamates from conserved pattern of cranial integration. *Proceedings of the National Academy of Sciences*, 116(29), 14688–14697. https://doi.org/10.1073/pnas.1820967116

Watanabe, A., Balanoff, A.M., Gignac, P.M., Gold, M.E.L., & Norell, M.A. (2021) Novel neuroanatomical integration and scaling define avian brain shape evolution and development. *eLife*, 10, e68809. https://doi.org/10.7554/eLife.68809

Weber, G.W., & Bookstein, F.L. (2011) *Virtual anthropology: a guide to a new interdisciplinary field*. Vienna: Springer Verlag, p. 423.

Webster, M., & Sheets, H.D. (2010) A practical introduction to landmark-based geometric morphometrics. *The paleontological society papers*, 16, 163–188. https://doi.org/10.1017/S1089332600001868

Weisbecker, V., Rowe, T., Wroe, S., Macrini, T.E., Garland, K.L., Travouillon, K.J., Black, K., Archer, M., Hand, S.J., Berlin, J.C., Beck, R.M.D., Ladevèze, S., Sharp, A.C., Mardon, K., & Sherratt, E. (2021) Global elongation and high shape flexibility as an evolutionary hypothesis of accommodating mammalian brains into skulls. *Evolution*, 75(3), 625–640. https://doi.org/10.1111/evo.14163

Zelditch, M.L., Swiderski, D.L., Sheets, H.D., & Fink, W.L. (2004) *Geometric morphometrics for biologists: A primer*. New York: Elsevier Academic Press, p. 483.

FIGURE CAPTIONS

Fig. 1. Schematic phylogenetic relationships of squamates sampled in the study (modified from Pyron et al. 2013; Singhal et al. 2021) associated with 3D renderings showing the crania of each species in lateral view and the endocast in dorsal (left) and lateral (right) views. Scale bars equal 2 mm. Coloured bones: Frontal (light green); Parietal (light blue); Orbitosphenoid (light red) Parabasisphenoid (dark blue); Supraoccipital (purple); Prootic (orange); Otoccipital (dark red); Basioccipital (dark green); Otoccipital complex (yellow).

Fig. 2. Endocast of *Lepidothyris fernandi* showing the location of the 20 newly-defined landmarks in (a) dorsal, (b) lateral and (c) ventral views. Scale bar equals 2 mm. Landmark definitions are given in Table 2.

Fig. 3. Sampling curves from performing LaSEC on the landmark-placement trials performed on *Blanus cinereus* (a, e), *Epicrates cenchria* (b, f), *Sphaerodactylus caicosensis* (c, g) and on the inter-specific dataset including one landmarking trial per specimen for each of the 10 different species (d, h) with respect to characterizing centroid size (a, b, c, d) and shape (e, f, g, h) variation. Each gray line indicates fit values from one iteration of subsampling. Thick, dark line denotes median fit value at each number of landmarks.

Fig. 4. Morphospace constructed from first two principal component (PC) axes of endocranial shape between *Blanus cinereus* (a, b), *Sphaerodactylus caicosensis* (e, f), and *Epicrates cenchria* (i, j). Digital endocasts are figured in dorsal (a, e, i) and lateral (b, f, j) views, and associated with heat plots representing the difference in landmark position between the two most extreme specimens along PC1 (c, d) and PC2 (g, h) in dorsal (c, g) and lateral (d, h) views.

Color reflects displacement magnitude (red/yellow = high/low displacement). Scale bars equal 2 mm.

Fig. 5. Morphospace constructed from first two principal component (PC) axes of endocranial shape between the ten squamate species. Digital endocasts of *Leposternon scutigerum* (a, b), *Sphaerodactylus caicosensis* (e, f), *Tropidurus torquatus* (g, h), and *Epicrates cenchria* (k, l), are figured in dorsal (a, e, g, k) and lateral (b, f, h, l) views. The heat plots represent the difference in landmark position between the two most extreme specimens along PC1 (c, d) and PC2 (i, j) in dorsal (c, i) and lateral (d, j) views. Color reflects displacement magnitude (red/yellow = high/low displacement). Scale bars equal 2 mm.

TABLE CAPTIONS

Table 1. List of the material analysed. Collection number: FS, Freshly dissected sample from specialized retailers; GD, Gheylen Daghfous personal collection; MS, Finnish Museum of Natural History; UF:herp, University of Florida Herpetology. Skull length (in mm) measured from the anterior end of the premaxillary to the posterior end of the basioccipital. Burrower and cryptozoic categories are defined as in Scanferla (2016).

Table 2. Landmark descriptions defined in the study

Table 3. Standard deviations (σ) for the three observers (MML, WK, and RA) and for pooled data calculated for *Blanus cinereus* (MS.1285). The ranks indicate which landmarks are most error-prone (low ranks) versus least error-prone (high ranks). The coefficient of variation (CV), calculated from the average distance for which the landmark is an endpoint, is reported for each landmark as a percentage. The values in boldface denote landmarks where either relative-error measure exceeds 5%.

Table 4. Standard deviations (σ) for the three observers (MML, WK, and RA) and for pooled data calculated for *Epicrates cenchria*. The ranks indicate which landmarks are most error-prone (low ranks) versus least error-prone (high ranks). The coefficient of variation (CV), calculated from the average distance for which the landmark is an endpoint, is reported for each landmark as a percentage. The values in boldface denote landmarks where either relative-error measure exceeds 5%.

Table 5. Standard deviations (σ) for the three observers (MML, WK, and RA) and for pooled data calculated for *Sphaerodactylus caicosensis* (UF:herp:95971). The ranks indicate which

landmarks are most error-prone (low ranks) versus least error-prone (high ranks). The coefficient of variation (CV), calculated from the average distance for which the landmark is an endpoint, is reported for each landmark as a percentage. The values in boldface denote landmarks where either relative-error measure exceeds 5%.

Table 6. Procrustes ANOVA for the hypothesis of covariation between endocast shape of *Blanus cinereus, Epicrates cenchria and Sphaerodactylus caicosensis* and the three factors tested (Observer, species, repetition). Significance test was based on 1000 iterations.

Table 7. Procrustes ANOVA for the hypothesis of covariation between endocast shape of all squamates studied here and the three factors tested (Group, habitat, allometry) without (*procD.lm*) and with (*procD.pgls*) consideration of phylogeny. Significance test was based on 1000 iterations.

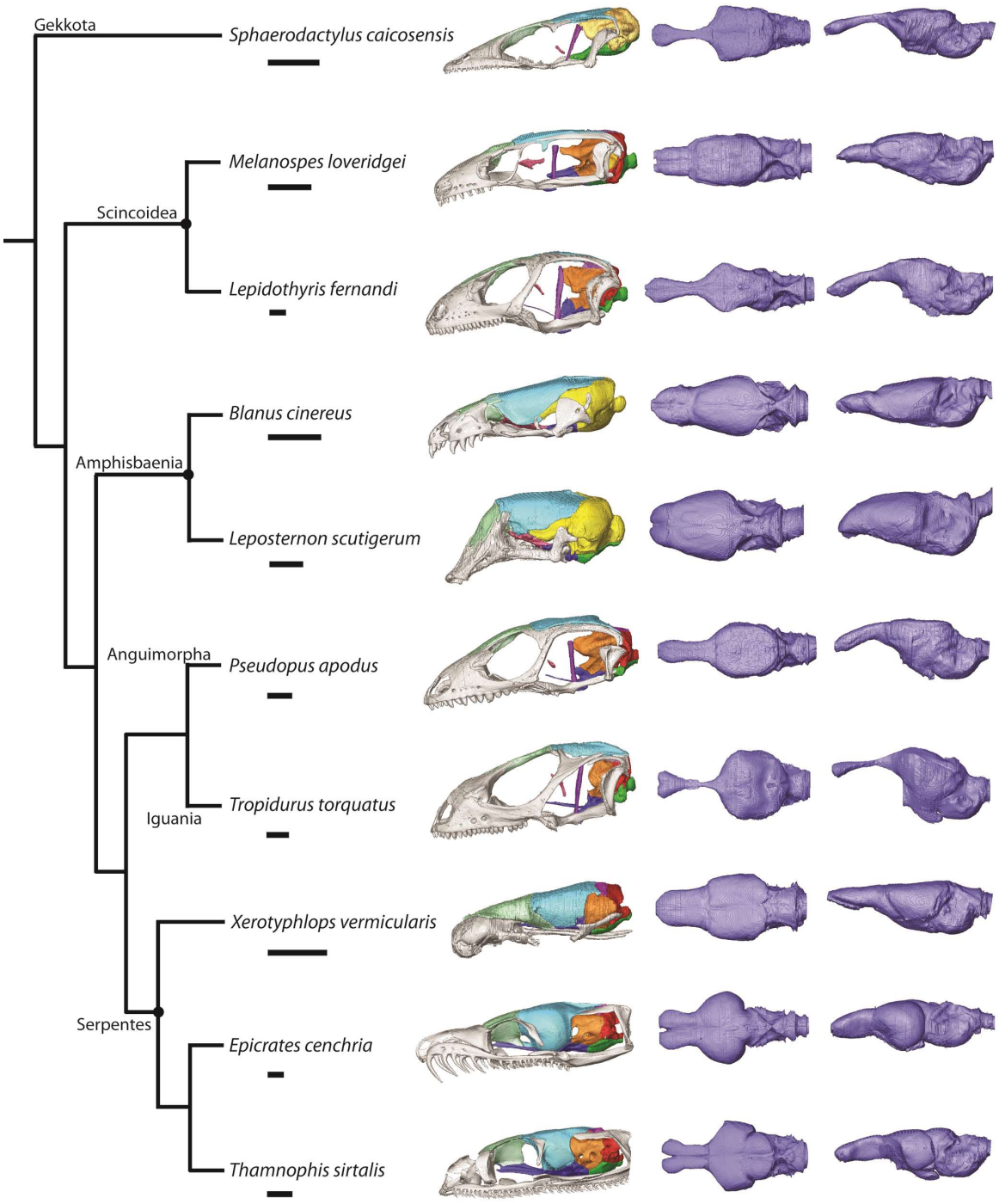
Gekkota
Sphaerodactylus caicosensis
Scincoidea
Melanospes loveridgei
Lepidothyris fernandi
Amphisbaenia
Blanus cinereus
Leposternon scutigerum
Anguimorpha
Pseudopus apodus
Iguania
Tropidurus torquatus
Serpentes
Xerotyphlops vermicularis
Epicrates cenchria
Thamnophis sirtalis

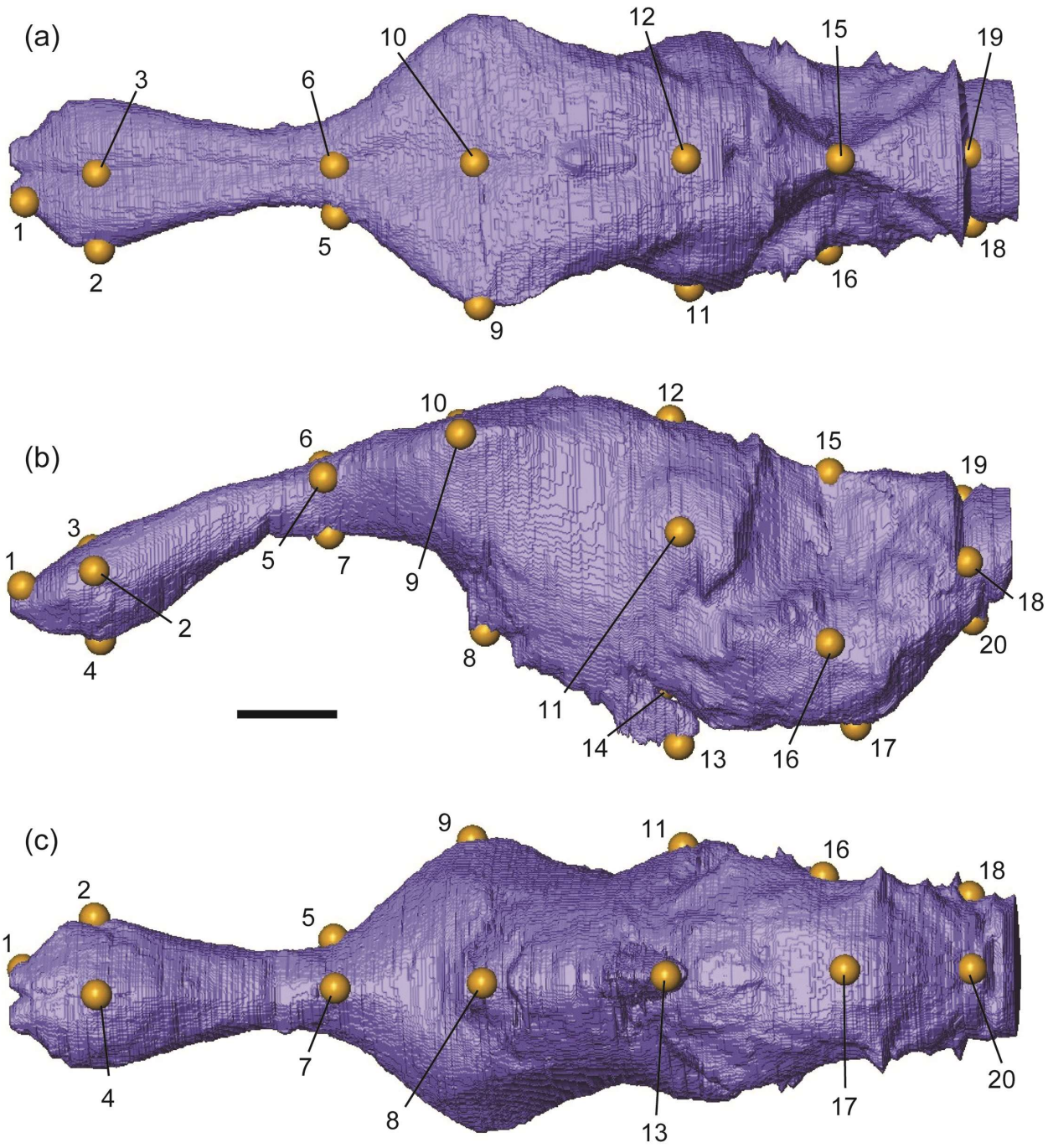
(a)
1
2
3
5
6
9
10
11
12
15
16
18
19
(b)
1
2
3
4
5
6
7
8
9
10
11
12
13
14
15
16
17
18
19
20
(c)
1
2
4
5
7
8
9
11
13
16
17
18
20

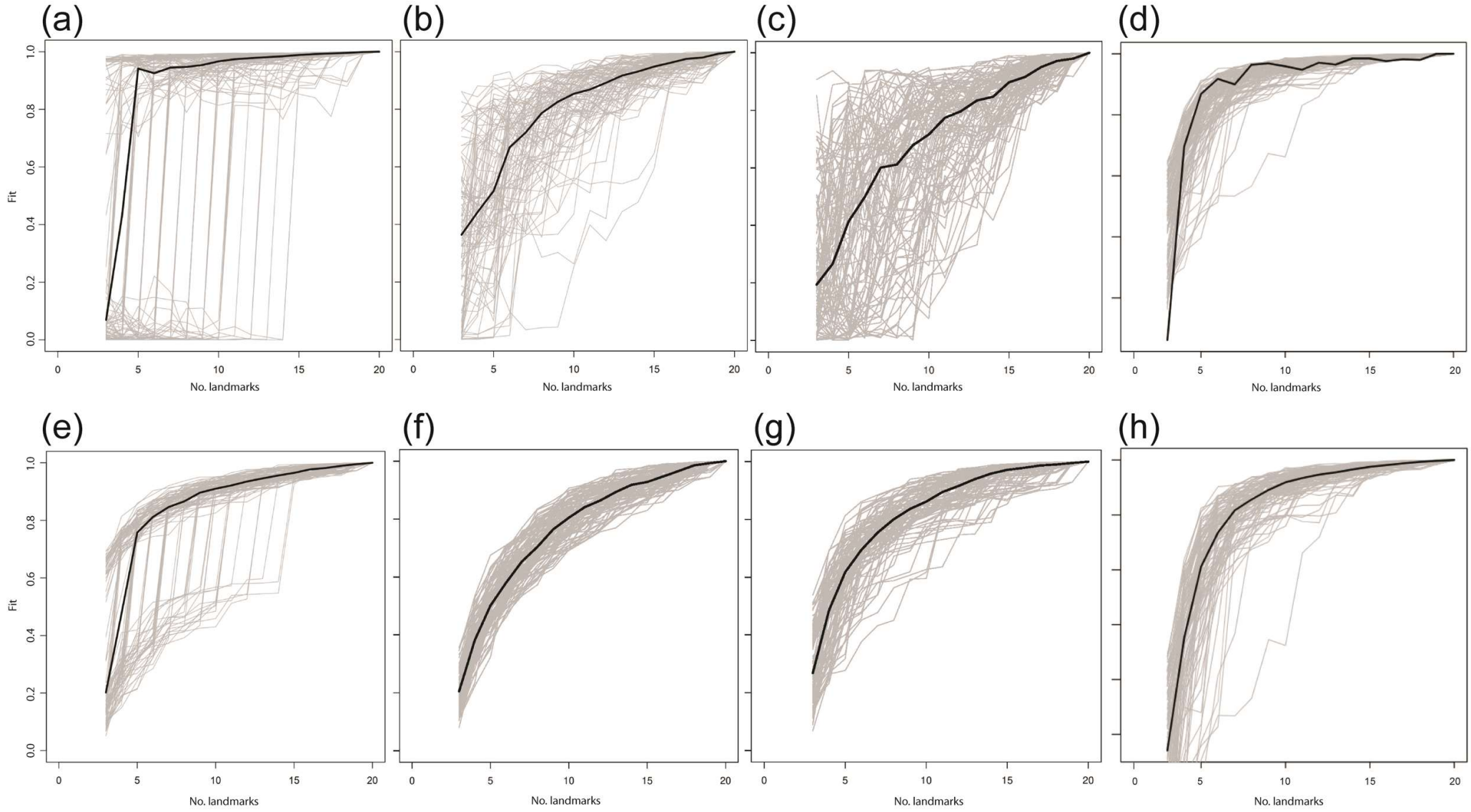
(a)
(b)
(c)
(d)
(e)
(f)
(g)
(h)
Fit
0.0
0.2
0.4
0.6
0.8
1.0
0
5
10
15
20
No. landmarks

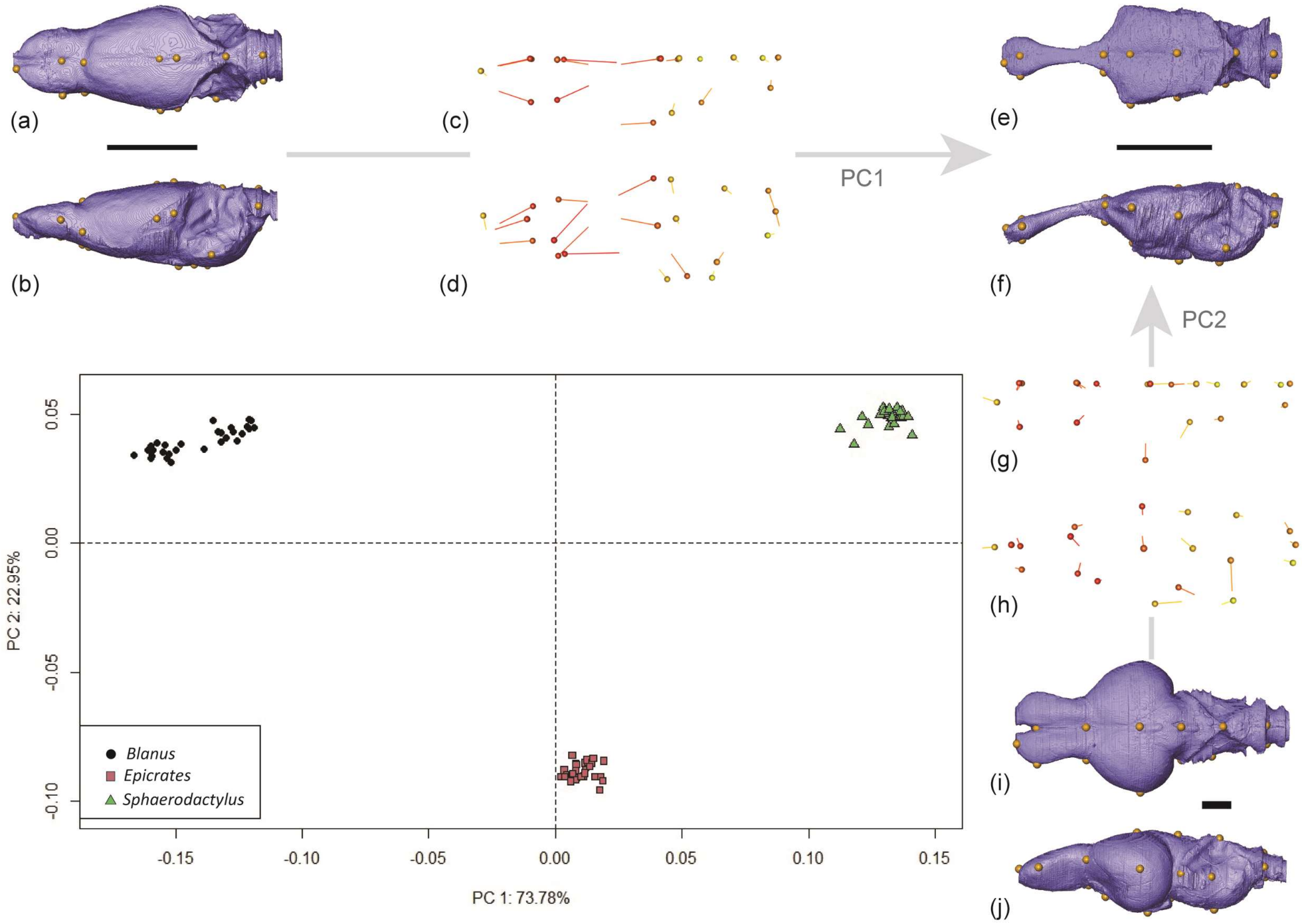
(a)
(b)
(c)
(d)
PC1
(e)
(f)
PC2
(g)
(h)
(i)
(j)
PC 2: 22.95%
PC 1: 73.78%
0.05
0.00
-0.05
-0.10
-0.15
-0.10
-0.05
0.00
0.05
0.10
0.15
Blanus
Epicrates
Sphaerodactylus

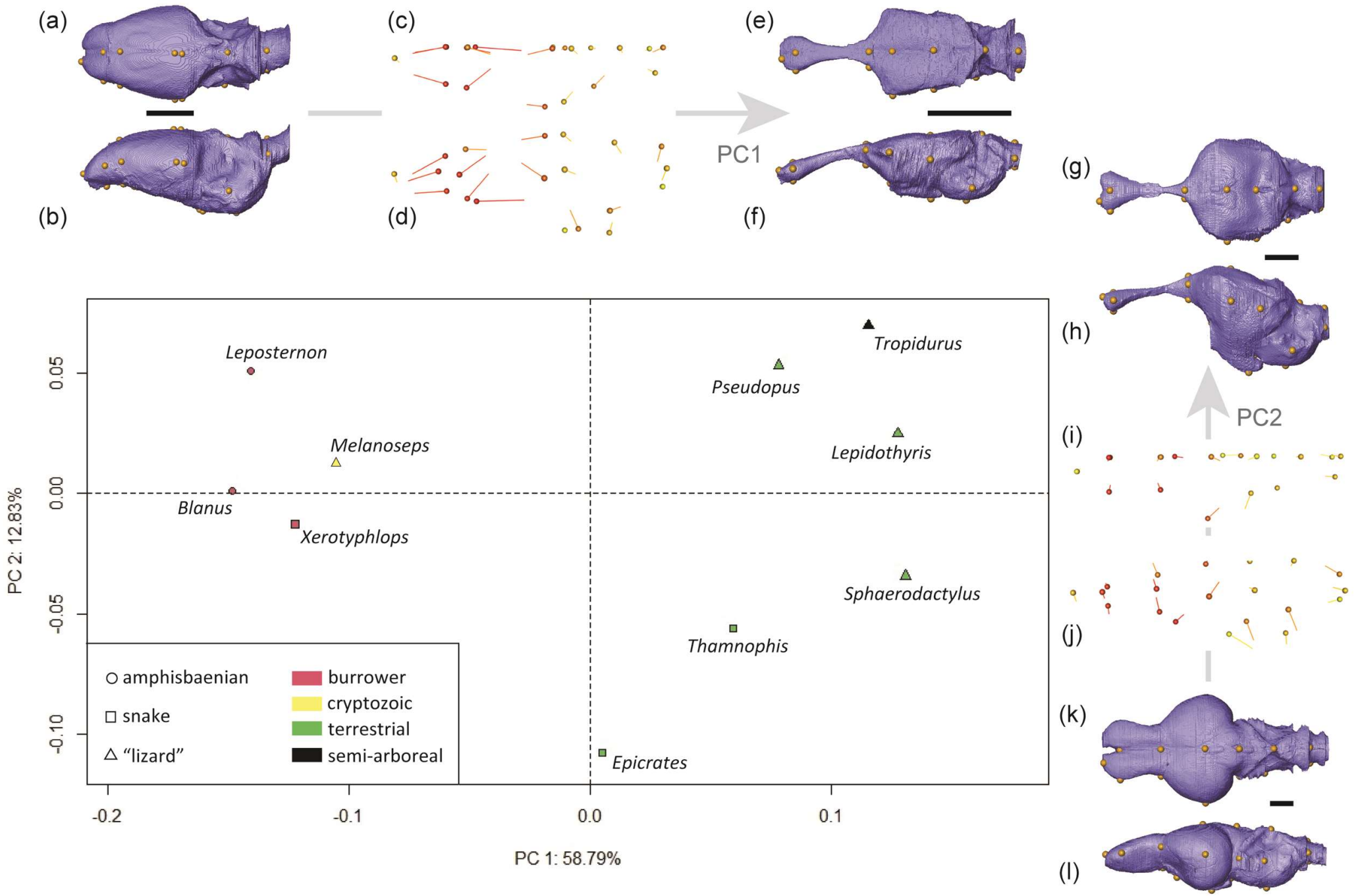
(a)
(b)
(c)
(d)
(e)
(f)
PC1
(g)
(h)
(i)
(j)
(k)
(l)
PC2
Leposternon
Melanoseps
Blanus
Xerotyphlops
Pseudopus
Tropidurus
Lepidothyris
Sphaerodactylus
Thamnophis
Epicrates
amphisbaenian
snake
"lizard"
burrower
cryptozoic
terrestrial
semi-arboreal
0.05
0.00
-0.05
-0.10
-0.2
-0.1
0.0
0.1
PC 2: 12.83%
PC 1: 58.79%

1 TABLE 1

Families	Species	Source	Collection number	Habitat modes	References	Skull length
Sphaerodactylidae	*Sphaerodactylus caicosensis*	Morphosource	uf:herp:95971	Terrestrial	Reynolds (2011)	7.6
Scincidae	*Melanoseps loveridgei*	Macri et al. (2019)	FS	Cryptozoic	Malonza and Bwong (2011)	9.6
Scincidae	*Lepidothyris fernandi*	Macri et al. (2019)	FS	Terrestrial	Akani et al. (2002)	24.1
Blanidae	*Blanus cinereus*	Macri et al. (2019)	MS.1285	Burrower	Gil et al. (1993)	7.5
Amphisbaenidae	*Leposternon scutigerum*	Macri et al. (2019)	MS.1196	Burrower	Kearney (2003)	10.5
Anguidae	*Pseudopus apodus*	Macri et al. (2019)	MS.1586	Terrestrial	Telenchev et al. (2017)	16.9
Tropiduridae	*Tropidurus torquatus*	Macri et al. (2019)	MS.1995	Semi-arboreal	Siqueira et al. (2013)	18.5
Typhlopidae	*Xerotyphlops vermicularis*	Macri et al. (2019)	MS.2033	Burrower	Afsar et al. (2016)	6.2
Boidae	*Epicrates cenchria*	Macri et al. (2019)	FS	Terrestrial	Andrade-Junior et al. (2020)	24.9
Colubridae	*Thamnophis sirtalis*	GD	GD Unnumb	Terrestrial	Burger et al. (2004)	14.5

2

TABLE 2

Number	Definition of landmarks
1	Anterior-most dorsal end of the endocast
2	Lateral-most extent of the cast of the olfactory bulbs and peduncles
3	Dorso-median extent of the cast of the olfactory bulbs and peduncles
4	Ventro-median extent of the cast of the olfactory bulbs and peduncles
5	Most lateral extent of the cast of the anterior cerebral hemispheres
6	Most dorso-median extent of the cast of the anterior cerebral hemispheres
7	Most ventro-median extent of the cast of the anterior cerebral hemispheres
8	Most ventro-median extent of the endocast at the posterior margin of the optic nerve foramen
9	Lateral-most extent of the cast of the cerebral hemispheres
10	Dorso-median extent of the cast of the cerebral hemispheres
11	Most lateral extent of the endocast at the anterior end of the anterior semicircular canal
12	Most dorso-median extent of the endocast at the anterior end of the anterior semicircular canal
13	Ventral most extent of the diencephalic cast
14	Cast of the mesencephalic flexure
15	Dorso-median extent of the endocast between the endosseous labyrinths
16	Lateral most extent of the endocast at the level of the endolymphatic foramen
17	Most ventro-median extent of the rhombencephalic cast
18	Lateral-most extent of the posterior end of the endocast
19	Most dorso-median extent of the posterior end of the endocast
20	Most ventro-median extent of the posterior end of the endocast

1 TABLE 3

Landmarks	MML			WK			RA			Pooled data		
	σ	**Rank**	**CV**	**σ**	**Rank**	**CV**	**σ**	**Rank**	**CV**	**σ**	**Rank**	**CV**
1	0.018	12	1.91%	0.006	20	0.67%	0.013	10	1.17%	0.023	12	2.27%
2	0.100	1	**11.96%**	0.061	1	**7.48%**	0.026	3	3.06%	0.087	1	**10.46%**
3	0.099	2	**13.06%**	0.060	2	**8.03%**	0.020	6	2.63%	0.085	2	**11.25%**
4	0.097	3	**12.24%**	0.059	3	**7.65%**	0.020	5	2.60%	0.084	3	**10.69%**
5	0.031	9	2.81%	0.013	12	1.18%	0.016	8	1.60%	0.024	11	2.25%
6	0.027	10	2.37%	0.013	13	1.13%	0.011	13	1.02%	0.021	13	1.92%
7	0.025	11	3.77%	0.011	15	1.58%	0.011	12	1.87%	0.021	14	3.22%
8	0.043	4	2.46%	0.017	9	0.99%	0.008	17	0.46%	0.034	7	1.99%
9	0.039	5	2.84%	0.031	6	2.31%	0.029	2	2.08%	0.039	5	2.84%
10	0.033	8	2.42%	0.023	7	1.67%	0.026	4	1.87%	0.031	9	2.27%
11	0.015	14	1.35%	0.039	4	3.38%	0.016	9	1.38%	0.035	6	3.04%
12	0.011	18	0.96%	0.006	19	0.56%	0.005	20	0.45%	0.009	18	0.81%
13	0.038	7	3.17%	0.018	8	1.57%	0.019	7	1.58%	0.032	8	2.70%
14	0.013	17	0.96%	0.010	16	0.74%	0.011	11	0.86%	0.013	16	1.01%
15	0.008	19	0.62%	0.007	17	0.49%	0.008	16	0.59%	0.008	20	0.60%
16	0.007	20	0.5%	0.007	18	0.48%	0.006	19	0.43%	0.009	19	0.66%
17	0.014	15	1.3%	0.013	11	1.14%	0.032	1	2.94%	0.027	10	2.46%
18	0.038	6	3.63%	0.036	5	3.71%	0.010	14	1.01%	0.048	4	4.79%
19	0.017	13	2.09%	0.014	10	1.75%	0.010	15	1.27%	0.014	15	1.78%
20	0.013	16	1.32%	0.012	14	1.20%	0.008	18	0.80%	0.013	17	1.33%

2

1 TABLE 4

Landmarks	MML			WK			RA			Pooled data		
	σ	Rank	CV	σ	Rank	CV	σ	Rank	CV	σ	Rank	CV
1	0.054	11	3.03%	0.064	6	3.56%	0.025	14	1.39%	0.059	13	3.29%
2	0.057	10	2.24%	0.043	13	1.71%	0.052	11	2.02%	0.059	12	2.33%
3	0.087	4	4.00%	0.060	8	2.73%	0.073	3	3.34%	0.076	7	3.49%
4	0.061	8	2.62%	0.053	11	2.25%	0.056	9	2.42%	0.062	10	2.66%
5	0.047	13	1.44%	0.032	16	0.98%	0.018	17	0.56%	0.060	11	1.84%
6	0.033	19	1.09%	0.027	18	0.88%	0.016	18	0.52%	0.044	17	1.43%
7	0.047	12	1.86%	0.037	15	1.47%	0.025	13	1.00%	0.055	15	2.18%
8	0.102	2	2.63%	0.093	1	2.42%	0.073	4	1.88%	0.098	3	2.52%
9	0.093	3	2.01%	0.071	4	1.57%	0.057	8	1.25%	0.088	5	1.91%
10	0.084	5	2.03%	0.065	5	1.58%	0.052	10	1.27%	0.074	9	1.80%
11	0.043	14	1.42%	0.054	10	1.84%	0.079	2	2.66%	0.150	1	**5.07%**
12	0.073	6	2.31%	0.026	19	0.80%	0.013	20	0.38%	0.055	14	1.71%
13	0.105	1	4.16%	0.039	14	1.51%	0.087	1	3.50%	0.084	6	3.36%
14	0.039	18	1.15%	0.023	20	0.69%	0.022	15	0.67%	0.037	19	1.12%
15	0.029	20	0.81%	0.048	12	1.36%	0.019	16	0.54%	0.035	20	0.99%
16	0.057	9	1.81%	0.080	2	2.60%	0.057	7	1.86%	0.108	2	3.49%
17	0.042	16	1.13%	0.061	7	1.62%	0.057	6	1.53%	0.075	8	2.00%
18	0.063	7	2.70%	0.078	3	3.40%	0.058	5	2.58%	0.095	4	4.14%
19	0.042	15	1.97%	0.058	9	2.67%	0.033	12	1.53%	0.051	16	2.39%
20	0.040	17	1.65%	0.031	17	1.24%	0.014	19	0.61%	0.039	18	1.61%

2

1 TABLE 5

Landmarks	MML			WK			RA			Pooled data		
	σ	**Rank**	**CV**	**σ**	**Rank**	**CV**	**σ**	**Rank**	**CV**	**σ**	**Rank**	**CV**
1	0.022	10	**5.30%**	0.011	9	2.45%	0.007	15	1.72%	0.022	9	**5.25%**
2	0.016	13	1.96%	0.010	12	1.19%	0.010	10	1.21%	0.014	14	1.67%
3	0.016	14	2.04%	0.007	15	0.93%	0.009	12	1.12%	0.012	16	1.49%
4	0.016	12	2.06%	0.009	13	1.09%	0.012	8	1.43%	0.014	13	1.70%
5	0.046	1	**5.08%**	0.023	2	2.59%	0.018	2	1.91%	0.044	2	4.82%
6	0.038	6	4.73%	0.017	5	2.11%	0.012	7	1.39%	0.036	4	4.43%
7	0.040	4	4.51%	0.018	4	1.93%	0.013	6	1.39%	0.038	3	4.19%
8	0.043	2	3.86%	0.035	1	3.08%	0.009	13	0.81%	0.051	1	4.59%
9	0.042	3	3.66%	0.014	6	1.25%	0.014	5	1.32%	0.036	5	3.18%
10	0.038	5	3.87%	0.007	17	0.69%	0.010	11	1.03%	0.026	8	2.66%
11	0.037	7	3.11%	0.023	3	1.96%	0.018	3	1.52%	0.029	6	2.52%
12	0.008	20	0.63%	0.006	18	0.55%	0.007	16	0.57%	0.007	20	0.62%
13	0.026	9	3.74%	0.011	7	1.67%	0.006	17	0.91%	0.021	10	3.11%
14	0.014	15	1.42%	0.008	14	0.87%	0.016	4	1.65%	0.028	7	2.91%
15	0.013	17	0.95%	0.010	11	0.76%	0.005	20	0.40%	0.010	18	0.77%
16	0.028	8	2.29%	0.007	16	0.58%	0.011	9	0.90%	0.021	11	1.70%
17	0.012	18	1.02%	0.011	10	0.91%	0.021	1	1.78%	0.017	12	1.46%
18	0.013	16	1.65%	0.011	8	1.40%	0.008	14	1.03%	0.011	17	1.44%
19	0.018	11	2.81%	0.004	20	0.64%	0.006	18	0.92%	0.012	15	1.83%
20	0.010	19	1.16%	0.006	19	0.72%	0.005	19	0.63%	0.010	19	1.17%

2

TABLE 6

Models	Df	*SS*	MS	Rsq	*F*	*Z*	*p*
Observer	2	0.006	0.003	0.004	4.705	2.520	0.006
Species	2	1.479	0.739	0.961	1147.259	14.269	0.001
Repetition	9	0.006	0.001	0.004	0.954	-0.117	0.534

TABLE 7

Models	Df	*SS*	MS	Rsq	*F*	*Z*	*p*
procD.lm							
Group	2	0.090	0.045	0.425	4.420	2.328	0.006
Habitat	2	0.070	0.035	0.332	3.445	2.003	0.013
Allometry	1	0.011	0.011	0.051	1.053	0.185	0.423
procD.pgls							
Habitat	2	0.38545	0.192726	0.4119	2.3748	1.50599	0.068
Allometry	1	0.0634	0.063402	0.06775	0.7812	0.07318	0.463